UNSTEADY SIMULATION OF TONAL NOISE FROM ISOLATED CENTRIFUGAL FAN

Martin OTTERSTEN[1,2], Huadong YAO[2], Lars DAVIDSON[2]

[1] *SWEGON AB, Box 336, 401 25 Gothenburg, Sweden*

[2] *CHALMERS University of Technology, Department of Mechanics and Maritime Science, Division of Fluid Dynamics, Horsalsvagen 7A Gothenburg, Sweden*

SUMMARY

In this study, an isolated centrifugal fan is investigated for the aerodynamic and acoustic performances using RANS and URANS simulations. The noise is predicted by coupling the URANS and the Ffowcs Williams and Hawkings acoustic analogy. The aerodynamic properties obtained from RANS and URANS are consistent with the experimental data. The magnitudes of the tonal noise at the blade passing frequencies are well predicted. Recirculating flows, which are responsible for reducing the fan efficiency and increasing the noise generation, are observed between the shroud and the blade trailing edges. It is found that the recirculating flows are associated with the gap between the shroud and the inlet duct.

INTRODUCTION

Isolated centrifugal fans are often used in ventilation systems and plays an important role in producing tonal and broadband noise. The broadband noise can be reduced when the fan efficiency is optimized. However, the tonal noise cannot be effectively reduced. It was reported that the dominating tonal noise occurs at blade passing frequencies (BPF) and that it is caused by the blade passing the volute tongue [1]. The tonal noise at the BPFs was also reported for an isolated centrifugal fan without a volute [2]. In a recent study [3], it was found that the dominant BPF tone is caused by the strong flow distortion at the fan inlet and flow separation at the blade foot. A filter was assembled in front of the inlet to decrease the tonal and broadband noise. In addition, a similar inlet setting was investigated [4]. It was reported that straightening inflow is effective for the noise reduction.

Numerical simulation is a more convenient way to identify tonal noise than experiments. However, simulation of the noise using advanced computational fluid dynamics (CFD) methods (e.g., large eddy simulation) requires many computational resources. To predict the tonal noise, a potentially

convenient method is the unsteady Reynolds Averaged Navier Stokes (URANS). The method can simulate characteristic unsteady structures, which are responsible for the tonal noise generation, with low computational costs. Though it has a drawback to provide the fluctuations that are important for the broadband noise generation.

The aim of this study is to investigate the tonal noise from an isolated centrifugal fan using the URANS methodology. A polyhedral mesh and a tetrahedral mesh will be compared in terms of the fan aerodynamic properties. The accuracy of the URANS to predict the tonal noise will be evaluated. The unsteady flow structures responsible for the tonal noise generated will be addressed.

CONFIGURATION

The isolated centrifugal fan is illustrated in Figure 1 and specified in Table 1. There is a gap between the stationary inlet duct and the rotating fan shroud. The numerical setup is in line with the experimental setup. The microphones/receivers are placed both upstream and downstream of the fan.

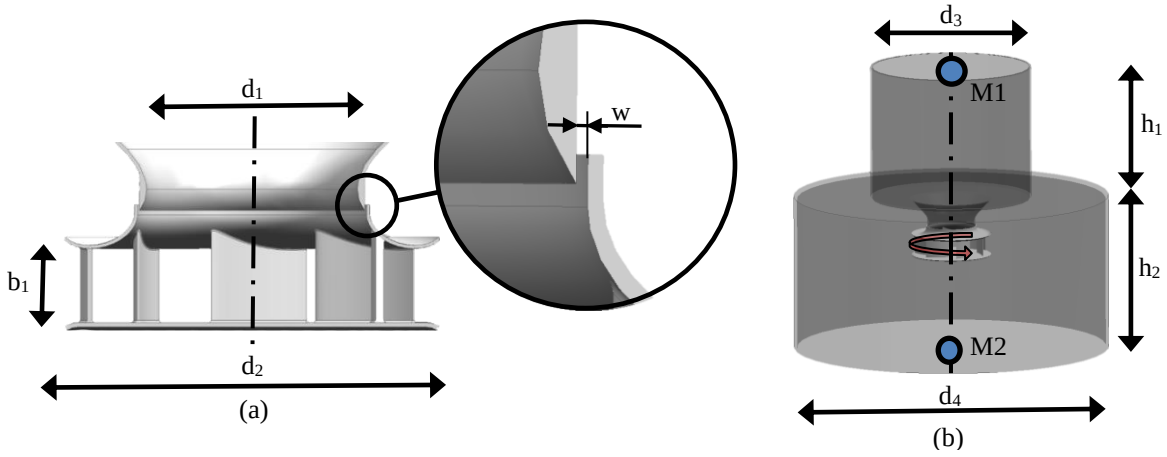

Figure 1: a) Impeller geometry b) Computational domain, where the microphones, M1 and M2, are marked

Table 1: Parameters of the fan.

Impeller diameter	d_2	0.268 m
Intake diameter	d_1	0.165 m
Fan width at d_2	b_2	0.053 m
Height inlet-region	h_1	0.4 m
Height outlet-region	h_2	0.5 m
Diameter inlet	d_3	0.6 m
Diameter outlet	d_4	1.1 m
Gap	w	0.0015 m
Number of blades	Z	7
Rotation speed	n	293.2 rad/s
BPF	BPF_0	326.7 Hz
BPF, first harmonics	BPF_1	653.4 Hz

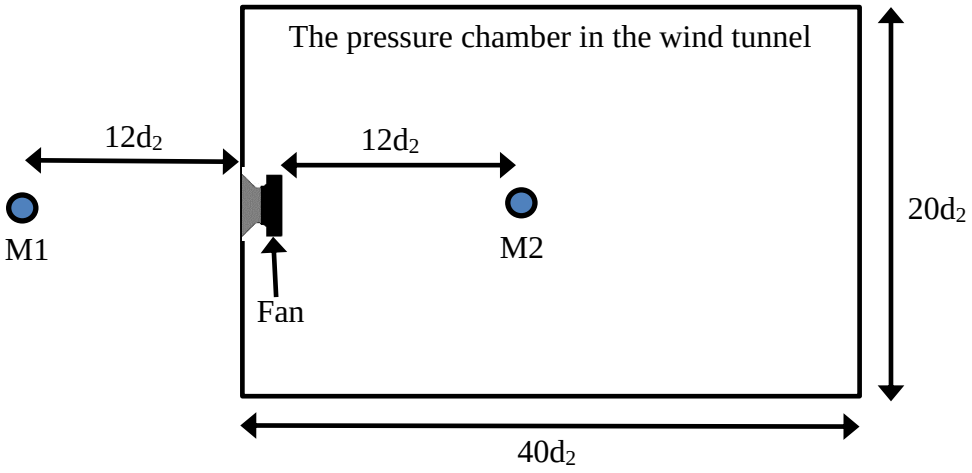

Figure 2: Experimental setup

NUMERICAL METHODOLOGY

The steady simulation

The Reynolds-averaged Navier-Stokes equation, RANS is used in the steady simulation. The finite volume method is used to discretize the continuity, momentum and energy equations. The turbulence model is the Realizable k-ε with enhanced wall treatment. It was found that the influence of the turbulence model on global performances of radial fan is minor in RANS [5]. The discretization scheme for the pressure is second-order. A second-order upwind scheme is used for the momentum and turbulent dissipation. The simulation is performed using the software ANSYS Fluent [6]. The coupled flow solver is used to solve the discretized equations.

The unsteady simulation

An incompressible URANS solver is applied to the unsteady simulation. The Mach number based on the tip velocity is 0.1. The incompressible flow assumption was made since the Mach number is low ($M < 0.3$) [7,8].

The turbulence model is the k-ω shear-stress transport (SST) [5,9]. The segregated flow solver is used to solve the discretized equations. The pressure-velocity coupling is calculated through the algorithm SIMPLEC (Semi-Implicit Method for Pressure-Linked Equations-Consistent). The SIMPLEC procedure is similar to the SIMPLE procedure. The only difference lies in the expression used for the face flux correction. The modified correction equation has been shown to accelerate convergence in problems where the pressure-velocity coupling is the main deterrent to obtain a solution [10]. The discretization scheme for the pressure is second-order. The momentum and turbulence kinetic energy are discretized with a second-order upwind scheme. The Kato-Launder formulation and production limiter is applied to avoid the excessive generation of the turbulence energy near stagnation points.

A second-order implicit method is used to discretize the time derivative, with inner iterations. It is the bounded second-order implicit method [10]. The fixed time step is set to $\Delta t = 5.95 \cdot 10^{-5}$ s. This gives a maximum Courant number of 66.

The constants for the SST model are the same as for the standard k-ω model and adopts the default values in the software. The SST k-ω model constants, $\sigma_{k,1} = 1.176$, $\sigma_{k,1} = 1.0$, $\sigma_{\omega,1} = 2.0$, $\sigma_{\omega,2} = 1.168$, $a_1 = 0.31$, $\beta_{i,1} = 0.075$ and $\beta_{i,1} = 0.0828$. The notations of the coefficients are the same as in the theory guide in Fluent [10].

The acoustic analogy

The incompressible flow solver can only solve the hydrodynamic pressure. The noise, which is the acoustic pressure, is excluded from the incompressible simulation. To predict noise, the Ffowcs Williams and Hawkings (FW-H) acoustic analogy is coupled with the URANS. The integral surface for the FW-H method is set on the blades, the backplate and the shroud (see Figure 3). A source region that is very small relative to its wavelength is said to be compact. Vortex characteristic length, $\mathcal{L}$, is estimated as the tip velocity divided by the maximum frequency. The wavelength, λ, is calculated as the speed of sound divided by the maximum frequency. So, $\mathcal{L} \gg \lambda$ and the source can therefore be treated as compact [11]. The ambient fluid for the FW-H method is set with the density of 1.225 kg/m^3, the speed of sound of 340 m/s and reference acoustic pressure of $2 \cdot 10^{-5}$ Pa.

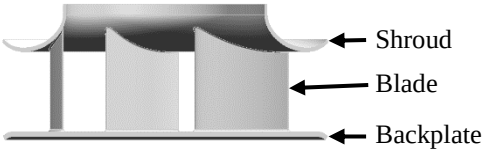

Figure 3: Illustration of the integral surfaces for the FW-H method

NUMERICAL SETTINGS

The computational domain for the simulation is illustrated in Figure 4. The fan-region is modelled with the sliding mesh technique. The rotating domain is fixed without an explicit rotating motion. The rotation is modelled by adding a rotating force term in the governing equations. With sliding mesh technique, the entire computational domain is divided into stationary and non-stationary domains with specific sliding interfaces between the domains. The physical quantities transporting between the domains are interpolated on the sliding interfaces. Since there is no modelling of the motion, the technique can handle problems with strong transient effects [10].

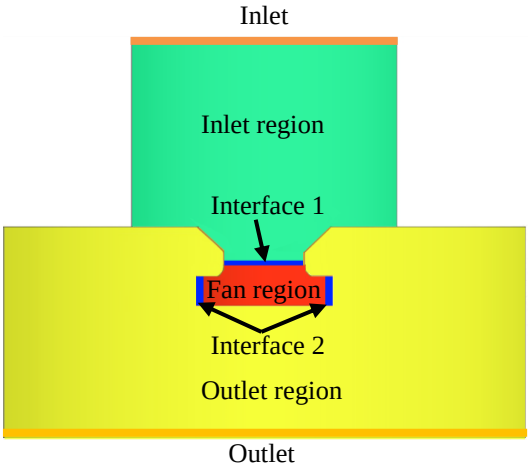

Figure 4: The fan region (red) is a rotating domain. The inlet region (green) and the outlet region (yellow) are non-rotating domains. The interfaces between the rotating and non-rotating domains are marked with blue

The frequency of the tones, BPF_0 and BPF_1, are 326.7 Hz and 653.4 Hz, respectively. The sampling frequency must be at least twice as high as the maximum frequency of interest (the Nyquist rate), this gives that $f_{max} \approx 1400\ Hz$. The acoustic simulation requires that $\Delta t < \Delta t_{calc}$. Δt is the selected time step and $\Delta t_{calc} = 1/(10 f_{max}) = 7.14 \cdot 10^{-5}\ s$. The selected time step fulfills this requirement. The frequency resolution should be half of the minimum frequency of interest, so $\Delta f \approx 160\ Hz$. The record time of signals is $T = 20/\Delta f = 0.2\ s$, which is approximately 10 rotation periods.

The mass-flow boundary condition is set at the inlet. The turbulence intensity, I, is set to 4%, according to $I = 0.16(R_e)^{-1/8}$ [10]. The turbulence length scale, ℓ, is set to the hydraulic diameter 0.05 m based on $\ell = 0.7d_{inlet}$, where d_{inlet} is the diameter of the inlet duct.

The pressure-outlet boundary condition with the Gauge pressure set to 0 Pa is set at the outlet. The non-slip boundary condition is used on the walls.

The under-relaxation factors for the momentum and the pressure in the segregated flow solver are set to 0.7 and 0.3 respectively. The under-relaxation factor for the turbulent kinetic energy is set to 0.8.

COMPUTATIONAL MESH

The simulations employ two meshes with different element types. One of them is constructed with tetrahedral elements and prism layers near the walls, whereas the other with polyhedral elements. The surface cell of the two meshes are shown in Figure 5. The interface between the outlet region and the rotating fan region is illustrated in Figure 6.

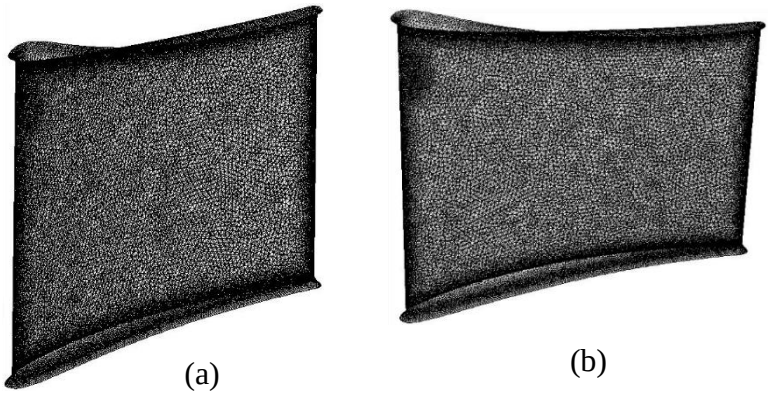

Figure 5: Surface mesh on the blade. a) Tetrahedral b) Polyhedral

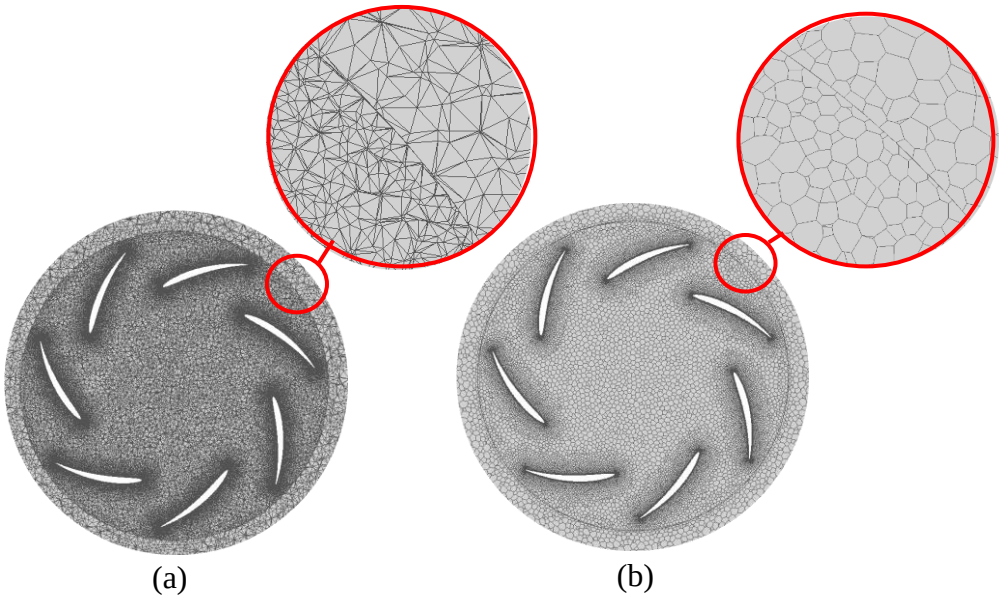

Figure 6: Volume mesh in a plane normal to the rotation axis. a) Tetrahedral b) Polyhedral

For the tetrahedral mesh, the maximum and minimum cell sizes on the blades are $8.2 \cdot 10^{-11}$ m^3 and $7.6 \cdot 10^{-13}$ m^3, respectively. On the shroud, the maximum and minimum cell sizes are $1.4 \cdot 10^{-10}$ m^3 and $1.1 \cdot 10^{-12}$ m^3, respectively. The maximum and minimum cell sizes in the rotating region are $1.6 \cdot 10^{-8}$ m^3 and $1.9 \cdot 10^{-13}$ m^3.

The polyhedral mesh generation method can control the growth ratio of cell size in the near field to small value. The growth rate is set to 1.05, as [12, 13]. The polyhedral mesh has the comparable cell size settings as the tetrahedral mesh. The maximum and minimum cell size in the rotating region are $1.2 \cdot 10^{-7}$ m^3 and $5.1 \cdot 10^{-14}$ m^3 respectively. In addition, the parameters of the mesh quality are presented in Table 2.

Table 2: Mesh data for tetrahedral and polyhedral mesh

	Tetrahedral	**polyhedral**
Number of nodes	3 503 692	16 132 851
Number of cells	12 489 406	8 366 763
Minimum Orthogonal Quality	0.151	0.165
Maximum Skewness	0.823	0.835
Maximum Aspect ratio	32.7	81.5
Y^+ near the walls in the rotating region	≤ 5	≤ 5

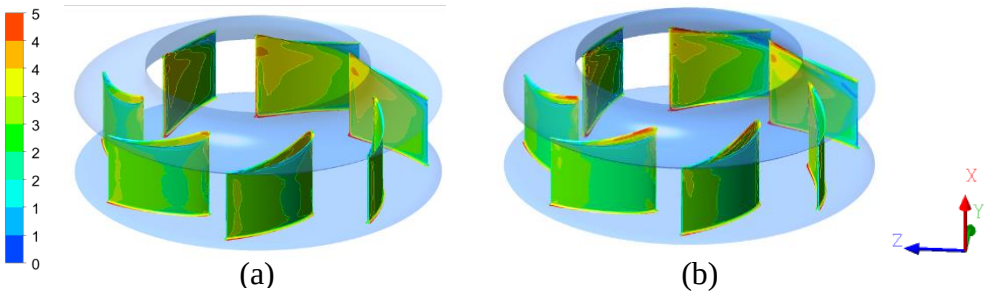

(a) (b)

Figure 7: y^+ near the blades. a) Tetrahedral, RANS b) Polyhedral, URANS

RESULTS AND DISCOUSSION

To check if the mass is conserved through the interfaces, the difference between the mass flow out from one region and the mass flow into the next region is calculated at interface 1 and 2, as which is illustrated in Figure 4. The results are presented in Table 3.

The important physical data for the fan was compared in Table 3. The results from the RANS and URANS simulation agree well with experimental data for both the tetrahedral and the polyhedral meshes, listed in Table 3. Contours of the static pressure and velocity magnitudes on the fan are showed in Figures 8 and 9. The statitc pressure on the blades and backplate are shown in Figure 10.

Table 3: Fan performance data, results from simulation and experiments

	RANS-Tetrahedral	**RANS-Polyhedral**	**URANS-Polyhedral**	**Experimental**
Flow rate (m^3/s)	0.398	0.398	0.398	0.395
Static pressure rise (Pa)	302.4	313.6	301.2	295.3
Torque (Nm)	1.276	1.247	1.235	1.234
Mass conservation interface 1 (kg/s)	$1.6 \cdot 10^{-16}$	$1.67 \cdot 10^{-16}$	$1.3 \cdot 10^{-16}$	-
Mass conservation interface 2 (kg/s)	$2.2 \cdot 10^{-15}$	$2.2 \cdot 10^{-15}$	0	-

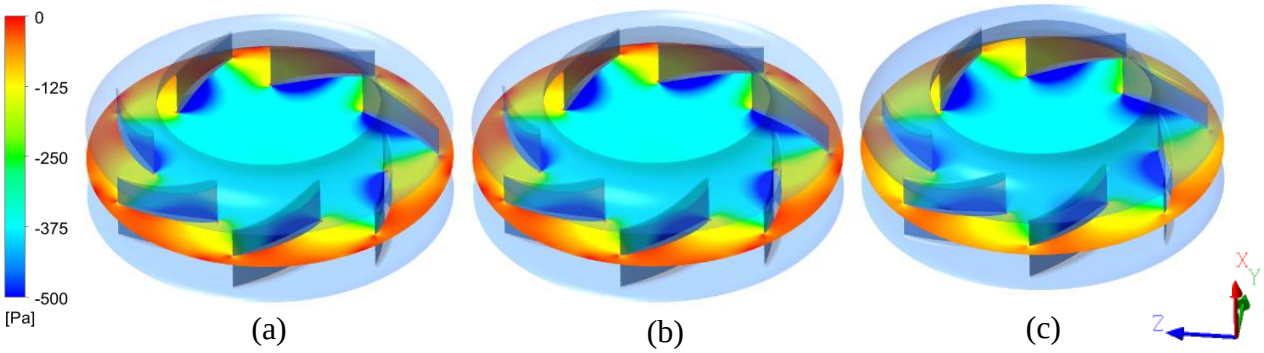

Figure 8: Static pressure in the fan region on a plane normal to the rotation axis a) RANS tetrahedral mesh b) RANS polyhedral c) URANS polyhedral mesh

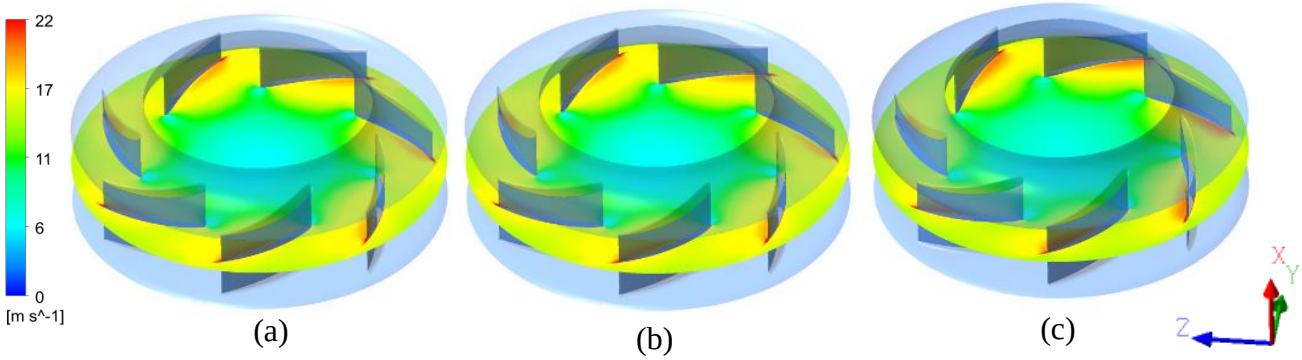

Figure 9: Velocity magnitude in the fan region on a plane normal to the rotation axis a) RANS tetrahedral mesh b) RANS polyhedral c) URANS polyhedral mesh

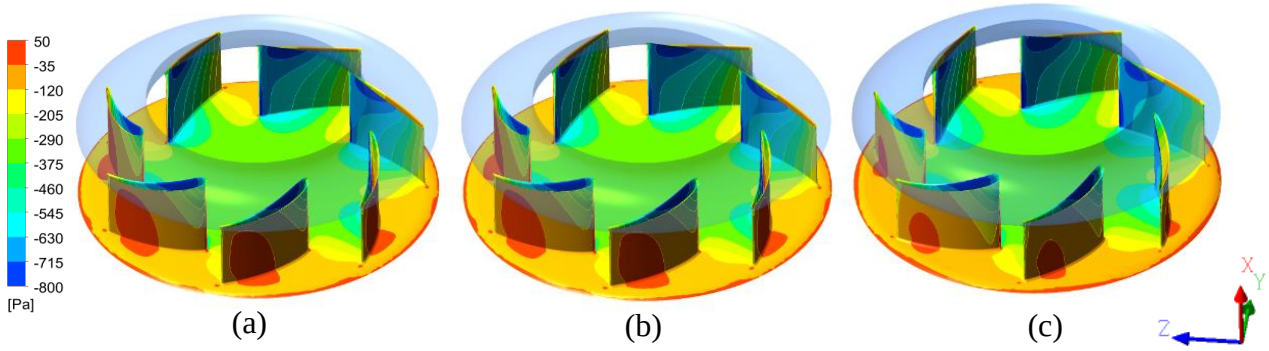

Figure 10: Static pressure on the blades and backplate. a) RANS tetrahedral mesh. b) RANS polyhedral mesh. c) URANS polyhedral mesh

The wall shear stress on the blade and streamlines are illustrated in figure 11. The fan performance is associated with the shear stress. Low shear stress is observed near the trailing edge of the blade. It is found that this is caused by the recirculated flow, which happens between the blade and the shroud. In addition, a small recirculation is seen between the backplate and fan trailing edge.

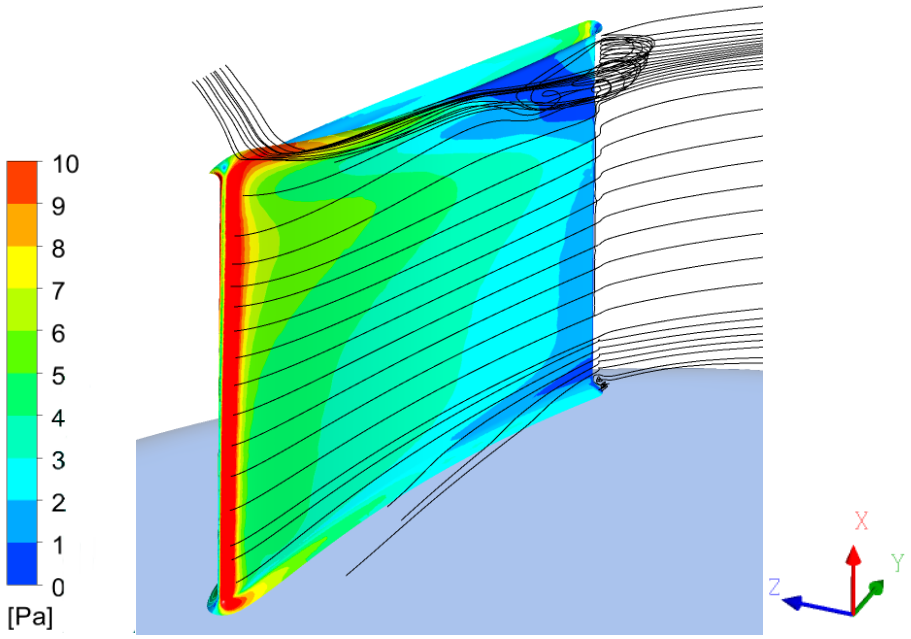

Figure 11: Contour plot of the wall shear stress at the blade with airflow visualized with streamlines

To get an improved understanding of the recirculated regions, the turbulence kinetic energy is illustrated in Figure 12. There is high turbulent kinetic energy in the region of the recirculated flow between the shroud and blade trailing edge. The turbulent kinetic energy is low at the small recirculation region close to the backplate. This high region of turbulent kinetic energy could be the dominant source for the noise generation.

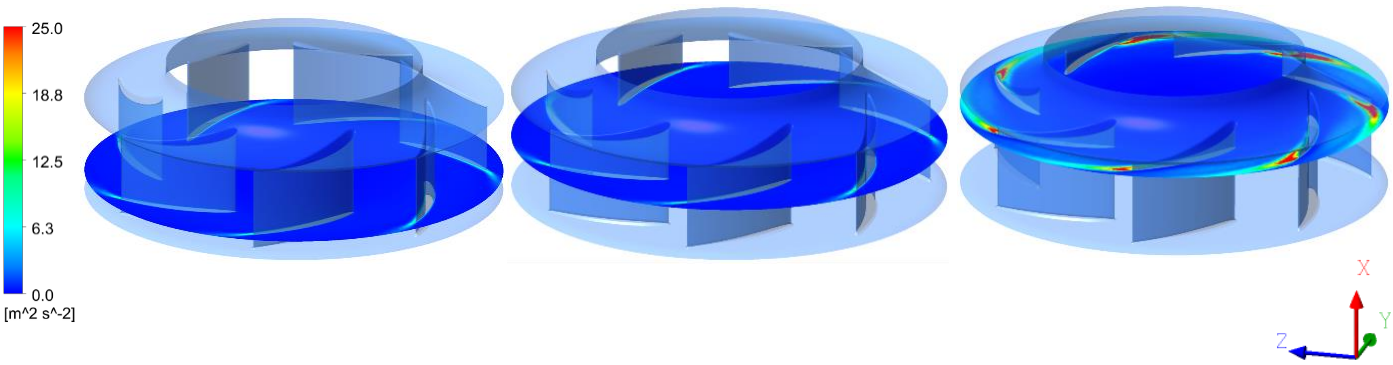

Figure 12: Turbulence kinetic energy on a plane normal to the rotation axis at different distance from the backplate

The flow around the shroud and blade are studied with streamlines in Figure 13. It is clear that the flow in the recirculated region comes from the gap. It could potentially influence the noise generation. In experiments, the same results were found, which are not present for the sake of brevity.

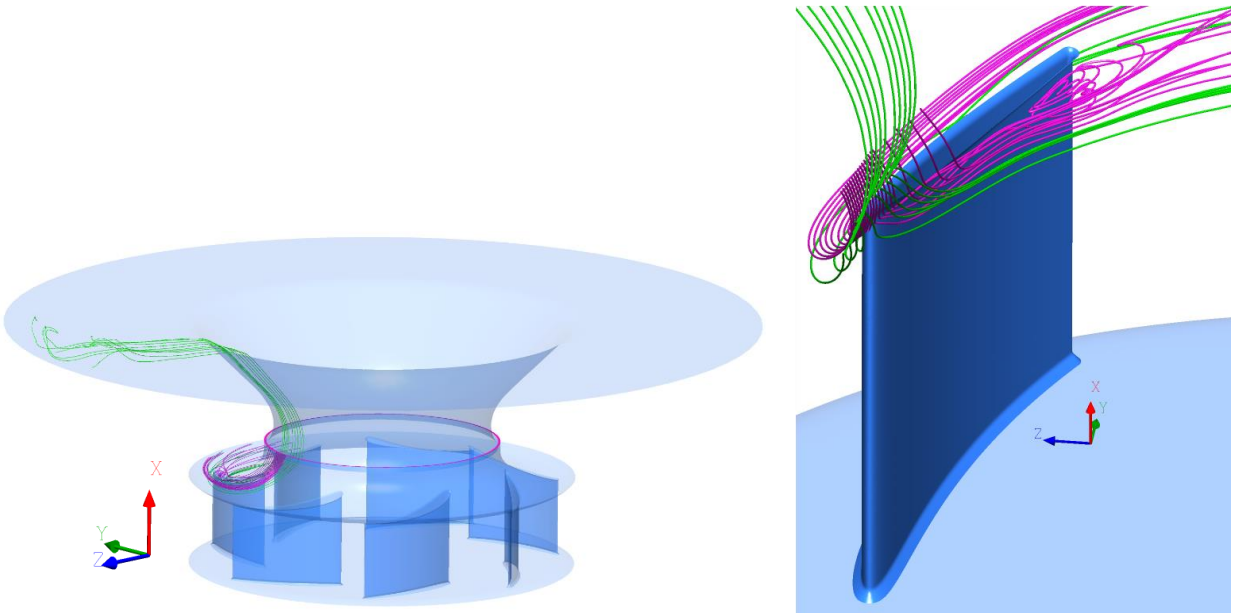

Figure 13: Streamlines from inlet (green) and from gap (pink)

The Power Spectral Density (PSD) of the noise at the microphones, M1 and M2 are shown in Figure 14. The tones measured at M1 agree well with the experimental result. At M2, the tones do not agree well. The noise characteristic can be affected by the flow through the fan [3,4]. The interaction between the noise and the resonance modes of the fan affects the magnitudes of the noise. This effect is more obvious near the outlet than the inlet. The same phenomenon is found in the experimental results. The broadband part of the spectra does not agree well with the experimental results. The reason is that the incompressible URANS cannot resolve the small fluctuations. Nonetheless, this method coupled with the FW-H method is efficient to predict the tonal noise, which is more important for quiet ventilation systems.

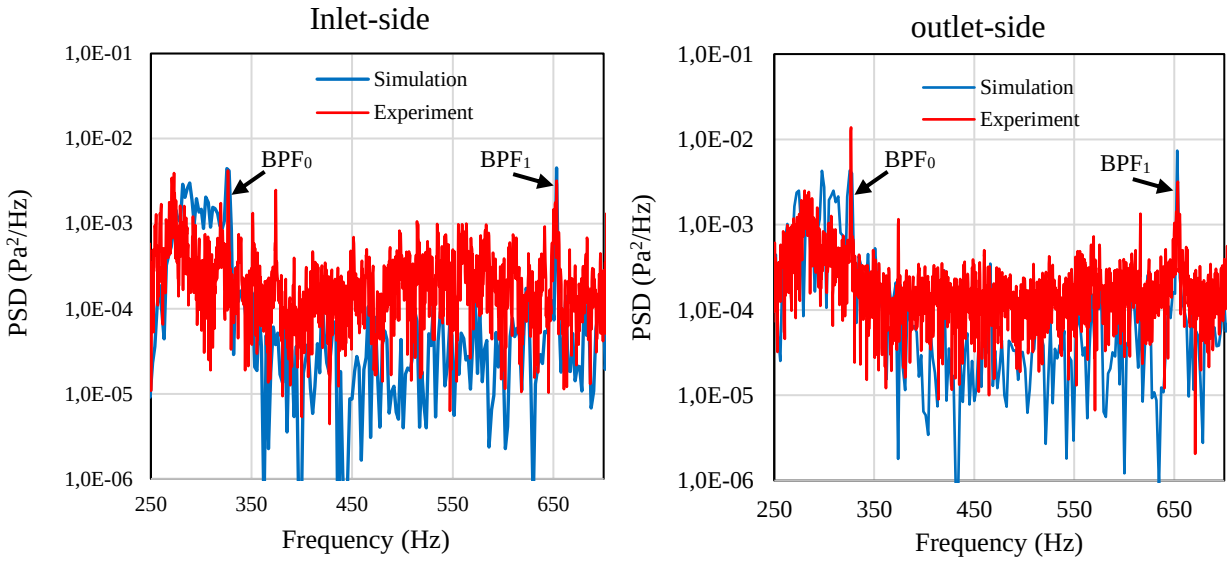

Figure 14: Comparison of Power Spectral Density at the inlet-side and at the outlet-side

CONCLUTION

The unsteady RANS simulation captures the tonal noise. The predicted BPF_0 tone agrees with the experimental data at the inlet-side. The spectra of the broadband noise below 350 Hz approximately agree with the experimental data. However, those at higher frequencies are underestimated since the small fluctuations are not resolved with this methodology. The tetrahedral and polyhedral meshes give comparable aerodynamic results, which agree with experimental data.

Recirculation is found at the pressure side of the blade close to the shroud. It is associated with the gap between the shroud and inlet duct. The recirculation flow can influence the fan efficiency and generate tonal noise. In addition, small recirculation is found on the pressure side of the blade close to the backplate.

REFERENCES

[1] Y. Otha, E. Outa, K. Tajima – *Evaluation and prediction of blade passing frequency noise generated by a centrifugal blower*. Journal of Turbomachinery vol. 118:597-605, **1996**

[2] D. Wolfram, T. H. Carolus – *Experimental and numerical investigation of the unsteady flow field and tone generation in an isolated centrifugal fan impeller*. Journal of Sound and Vibrations vol. 329: 4380-4397, **2010**

[3] M. Sanjose, S. Moreau – *Direct noise prediction and control of an installed large low-speed radial fan.* European Journal of Mechanics vol. 61:235-243, **2017**

[4] A. Lawrenson, G. Berg, C. Carlsson, M. Fransson, L. All, inventors; Swegon AB, applicant. – *Low profiled AHU with tilted rotary heat exchange*. International patent WO 2010085197, **2010**

[5] M. Sanjose, S. Moreau – *Numerical simulations of a low-speed radial fan*. Int. J. Engineering Systems Modelling and Simulation, vol. 4, Nos. ½, pp.47-58, **2012**

[6] Ansys Inc. – *Fluent User Guide*. Version 17.2, **2017**

[7] M. Younsi, F. Bakir, S. Kouidri, R. Rey – *Numerical and experimental study of unsteady flow in a centrifugal fan*. Journal of Power and Energy, 221(7):1025-1036, **2007**

[8] Q. Liu, D. Qi, Y. Mao – *Numerical calculation of centrifugal fan noise*. Proceedings of the Institution of Mechanical Engineers, 220(C8):1167-1177, **2006**

[9] J.E. Bardina, P.G. Huang and T.J. Coakley – *Turbulence modelling validation, testing and development*. Technical report, NASA TM-110446, **1997**

[10] Ansys Inc. – *Fluent Theory Guide*. Version 17.2, **2017**

[11] M. E. Goldstein – *Aeroacoustics*. McGraw-Hill, page 34-37, **1976**

[12] H. D. Yao, L. Davidson. L. E. Eriksson – *Surface integral analogy approaches for predicting noise from 3D high-lift low-noise wings*. Acta Mech. Sin. 30(3):326-338, **2014**

[13] H. D. Yao, L. Davidson. L. E. Eriksson – *Noise Radiated by Low-Reynolds Number Flows past a Hemisphere at Ma=0.3*. Phys. Fluids 29(7):076102, **2017**